Article ID: 1006-8775(2023) 01-0101-14

Moisture Transport and Associated Background Circulation for the Regional Extreme Precipitation Events over South China in Recent 40 Years

YANG Wen-ting (杨雯婷)[1, 2], FU Shen-ming (傅慎明)[3], SUN Jian-hua (孙建华)[1, 2, 4],
WANG Hui-jie (汪汇洁)[1], FU Ya-nan (付亚男)[1, 2], ZENG Chui-kuan (曾垂宽)[5]
(1. Laboratory of Cloud-Precipitation Physics and Severe Storms, Institute of Atmospheric Physics, Chinese Academy of Sciences, Beijing 100029 China; 2. University of Chinese Academy of Sciences, Beijing 100049 China;
3. International Center for Climate and Environment Sciences, Institute of Atmospheric Physics, Chinese Academy of Sciences, Beijing 100029 China;
4. Southern Marine Science and Engineering Guangdong Laboratory (Zhuhai), Zhuhai, Guangdong 519000 China;
5. China Resources Power Technology Research Institute Co., Ltd, Shenzhen, Guangdong 518000 China)

Abstract: Based on the hourly precipitation data at 176 observational stations over south China and the hourly ERA5 reanalysis data during the 40-yr period of 1981-2020, we analyzed the universal characteristics of moisture transport and their associated background circulations for four types of regional extreme precipitation events (REPEs) over south China. Main findings are shown as follow. (i) The wind that transported moisture for the REPEs over south China featured a notable diurnal variation, which was consistent with the variations of the precipitation. (ii) Four types of REPEs could be determined, among which the southwest type (SWT) and the southeast type (SET) accounted for ~92% and ~5.7%, respectively, ranking the first and second, respectively. (iii) Trajectory analyses showed that the air particles of the SWT-REPEs had the largest specific humidity and experienced the most intense ascending motion, and therefore their precipitation was the strongest among the four types. (iv) South China was dominated by notable moisture flux convergence for the four types of REPEs, but their moisture transport was controlled by different flow paths. (v) Composite analyses indicated that the background circulation of the four types of REPEs showed different features, particularly for the intensity, location and coverage of a western Pacific subtropical high. For the SWT-REPEs, their moisture transport was mainly driven by a lower-tropospheric strong southwesterly wind band in the low-latitude regions. Air particles for this type of REPEs mainly passed over the Indochina Peninsula and South China Sea. For the SET-REPEs, their moisture transport was mainly steered by a strong low-tropospheric southeasterly wind northeast of a transversal trough. Air particles mainly passed over the South China Sea for this type of REPEs.

Key words: regional extreme precipitation event; south China; moisture transport; composite analysis; backward tracking analyses

CLC number: P434.5 **Document code:** A

Citation: YANG Wen-ting, FU Shen-ming, SUN Jian-hua, et al. Moisture Transport and Associated Background Circulation for the Regional Extreme Precipitation Events over South China in Recent 40 Years [J]. Journal of Tropical Meteorology, 2023, 29(1): 101-114, https://doi.org/10.46267/j.1006-8775.2023.008

1 INTRODUCTION

Under the global warming, in many regions of the world, extreme precipitation events have increased significantly, particularly for China (Li et al. [1]; Fu et al. [2]; Alexander [3]; Wang et al. [4]). This resulted in more frequent and stronger mountain torrents, debris flows, urban water loggings and other related disasters, which posed a great threat to the natural environment, human society and economy (Alexander [3]; Cheng et al. [5]). As the moisture is a necessary condition for the rainfall (Cao et al. [6]; Zhang et al. [7]; Wang et al. [8]; Zhuang et al. [9]), for decades, numerous studies have been conducted to further the understanding of the moisture transport features (Zhou et al. [10]; Zhang et al. [11]; Li et al. [12]; Lin et al. [13]). Related studies can be roughly divided into two groups. (i) The overall effects of the moisture transport on the precipitation of a large region during a relatively long period. For instance, Zhou and Yu [14] found that when abnormally more precipitation appeared over east China in summer, abnormal moisture was transported from the western Pacific to the South China Sea. Shen et al. [15] examined the moisture transport for the rainfall over east China in summer, and found that the anomalous moisture transport was mainly due to the northerly wind associated with a cold trough in north China and a southeast monsoonal wind to the south of the Western Pacific Subtropical High (WPSH). Hu et al. [16] analyzed the interdecadal characteristics of

Received 2022-09-21; **Revised** 2022-11-15; **Accepted** 2023-02-15

Funding: National Key Research and Development Program of China (2019YFC1510400); National Natural Science Foundation of China (42075002)

Biography: YANG Wen-ting, Ph. D., primarily undertaking research on mesoscale meteorology.

Corresponding author: SUN Jian-hua, email: sjh@mail.iap.ac.cn

the moisture transport over East Asia in summer, and found that an abnormal zonal moisture transport dominated the decadal variation of the moisture flux over northern East Asia during the late 1990s. Hu et al. [17] proposed that the intensity and frequency of extreme precipitation over most of east China tended to increase when the moisture transported from this part of China became stronger and meanwhile the moisture transported from the Northwest Pacific became weaker. (ii) The specified effects of the moisture transport on the regional extreme precipitation events (REPEs). For example, Mao et al. [18] analyzed the characteristics of moisture transport of a REPE in Zhejiang province in June 2016, and found that a southwesterly jet stream from the South China Sea transported abundant moisture to the rainfall region. Wang et al. [19] examined the characteristics of the moisture of a REPE in Chengdu, and found that the moisture transport was mainly driven by the high- and low-level jet streams associated with the typhoon Hagupit.

As one of the three major rain zones in China (south China, north China and the Yangtze River Basin; Tao [20]), south China features complicated terrain and land use (e.g., the Yunnan-Guizhou Plateau in its west, the tropical ocean to its southeast), which provide favorable conditions for the frequent occurrence of the REPEs (Zhao et al. [21]; Tan et al. [22]; Chen et al. [23]). As 97% of the total annual precipitation in south China is caused by the moisture imported from abroad (Wang et al. [24]; Yu et al. [25]; Li et al. [26]), investigating the key features of the moisture transport for REPEs in this region is of great importance. Previous studies suggested that the Pacific, the South China Sea and the Bay of Bengal served as important moisture sources for the REPEs over south China. Hu et al. [27] evaluated 13 REPEs in south China from mid-March to early May, and found that the moisture sources of these events were mainly located over the South China Sea and the tropical Pacific. Ji et al. [28] found that the Western Pacific and the Bay of Bengal acted as the main moisture sources for the REPEs in Guangdong during the annually first rainy season (April to June).

However, most previous studies mainly focused on the characteristics of the moisture transport for the REPEs over south China by conducting case studies. As a result, the universal features of these events remained unclear. Based on previous studies, the primary goal of the present study is to show the universal characteristics of the moisture transport of the REPEs over south China, and to explore the key features of their associated background circulation. Recently, Yang et al. [29] had proposed that the REPEs which lasted for 2−3 days occupied a proportion of 91% of all the persistent REPEs in south China, and their intensity were generally stronger than the REPEs persisting for 4−5 days. Therefore, in this study, we mainly focused on the REPEs with a duration of 2−3 d, which were representative for the REPEs over south China effectively. The present study is based on the result of Yang et al. [29], which selected REPEs and then analyzed their temporal and spatial characteristics. The remaining of this article is organized as follows: Section 2 describes the data and methods, sections 3−4 present the features of the moisture transport and the background circulation, and section 5 provides the discussion and conclusion.

2 DATA AND METHODS

A total of three types of data were used in this study: (i) the 2-d and 3-d typhoon-free REPEs from May to September during 1981−2020 (Table 1), which were provided by Yang et al. [29]; (ii) the hourly precipitation data at 176 observational stations over south China (i.e., Guangdong and Guangxi) (Fig. 1); and (iii) the hourly, 0.25° × 0.25° ERA5 reanalysis data (including geopotential height, temperature, specific humidity, potential temperature, zonal wind and meridional wind) from the European Centre for Medium-Range Weather Forecasts (ECMWF) (https://cds. climate. copernicus. eu/) (Hersbach et al. [30]).

The trajectory model HYSPLIT V4.9 provided by the National Oceanic and Atmospheric Administration (NOAA) Air Resources Laboratory (Stein et al. [31]) was used to analyze the moisture sources of REPEs. The advection and diffusion calculation of this model adopted the Lagrange method, which was usually used to track the movement trajectory of particles carried by the airstream. Furthermore, the influence of terrain was considered when tracking. This model used the ERA5 reanalysis data as input. In this study, the calculating area was 20°N−27°N, 104.5°E−118.0°E, which was used to represent south China (Fu et al. [2]). In the vertical direction, three levels (2200 m, 2000 m and 1700 m) were selected as the initial heights of the backward tracking. These three levels were determined by the relationship between wind speed at different altitudes and the variation of the precipitation (section 3.2). The backward tracking was started at 0000 UTC and 1200 UTC every day during all the REPEs by using a total of 528 points (176 at each vertical level) that covered south China. For instance, for a 2-d REPE, we conducted the backward tracking four times (i. e., at 0000 UTC and 1200 UTC on the first day and second day). Thus, there were 528 × 4 trajectories for this event. All backward tracking were calculated in a 72-h time window (i. e., from the initial time to 72 h earlier).

In order to capture the key characteristics of a REPE, there were mainly three processing steps during the analysis of moisture transport. Step 1: The REPE's associated trajectories (2-d REPEs with a total of 528×4 trajectories, and 3-d REPEs with a total of 528 × 3 trajectories) were clustered into different groups according to the principle of nearest grouping by using the cluster analysis method (Stein et al. [31]). Step 2: The

Table 1. All typhoon-free REPEs (66 two-day events and 21 three-day events) identified in this study from May to September during 1981–2020.

2-d REPEs			3-d REPEs
9–10 May 1981	23–24 Jun 1998	23–24 May 2009	28–30 Jun 1981
28–29 Sep 1981	23–24 Jun 1998	31 May –1 Jun 2010	10–12 May 1982
28–29 May 1982	23–24 Jul 1998	11–12 May 2011	16–18 Jun 1983
17–18 Aug 1982	9–10 Jun 2000	28–29 Jun 2011	29 Jun–1 Jul 2002
17–18 May 1984	24–25 May 2001	28–29 Jun 2011	18–20 Jul 2002
30–31 May 1984	16–17 Jul 2001	15–16 May 2013	18–20 Jul 2004
10–11 May 1986	1–2 Jun 2002	22–23 May 2014	5–7 Jun 2005
4–5 Jul 1986	14–15 Jun 2002	12–13 Aug 2014	25–27 May 2006
15–16 May 1987	19–20 Jul 2002	19–20 May 2015	7–9 Jun 2007
20–21 May 1987	16–17 May 2003	20–21 Jul 2015	5–7 Jun 2008
29–30 Jul 1987	9–10 Jun 2003	26–27 Jul 2015	11–13 Jun 2008
9–10 Aug 1991	26–27 Jun 2003	19–20 May 2016	15–17 Jun 2008
7–8 Jun 1992	14–15 Sep 2003	11–12 Jun 2016	6–8 Jul 2008
16–17 Jun 1992	11–12 May 2004	14–15 Jun 2016	2–4 Jul 2009
8–9 Jun 1993	20–21 Jun 2005	9–10 Sep 2016	14–16 Jun 2010
7–8 Jul 1993	21–22 May 2006	22–23 Jun 2018	21–23 Jun 2012
15–16 May 1994	8–9 Jun 2006	29–30 Aug 2018	19–21 May 2013
26–27 Jun 1995	7–8 Jun 2007	26–27 May 2019	4–6 Jun 2014
3–4 Aug 1995	7–8 Jun 2007	9–10 Jun 2019	16–18 Jun 2017
28–29 Jun 1996	13–14 Aug 2007	12–13 Jul 2019	1–3 Jul 2017
16–17 Jul 1996	8–9 Jun 2008	20–21 May 2020	6–8 Jul 2019
7–8 Jul 1997	16–17 May 2009	24–25 Jun 2020	

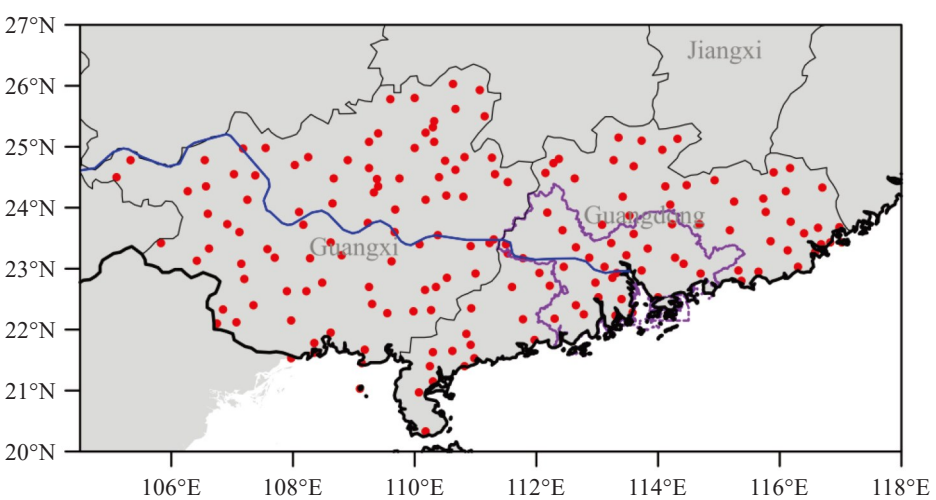

Figure 1. Distribution of 176 observational stations over south China used in this study. The Greater Bay Area was outlined in purple.

clustering results of each REPE were further divided into the southwest, northwest, northeast, and southeast types (i.e., SWT, NWT, NET, and SET) according to the directions of trajectories (SWT: 180°–270°; NWT: 90°–180°; NET: 0°–90°; SET: 270°–360°). It should be noted that the word 'types' here were different from the word 'groups' in Step 1. Step 3: For each REPE, we compared the moisture contribution rates of the SWT, NWT, NET, and SET, and determined the largest rate. This largest moisture contribution rate was used to classify the type of REPEs: for those to which the SWT moisture transport made the largest contribution, they were defined as the SWT-REPE, etc. In this study, the method documented in Sun et al. [32], which took the variation of the moisture during the movement into account, was used to calculate the moisture contribution rates of the moisture of different trajectories. Its expression is shown as in Eq. (1):

$$Q_{all} = \left(\sum_{1}^{m} \sum_{it=1}^{72} q_{it} / \sum_{1}^{n} \sum_{it=1}^{72} q_{it} \right) \times 100\% \quad (1)$$

where m is the number of the trajectories contained in a single cluster, n represents the total number of the trajectories for all clusters, it represents the backward tracking time, and q_{it} is the specific humidity of the air mass at each time during the whole backward tracking time.

3 OVERVIEW OF THE SELECTED REPEs

3.1 *Intensity and frequency*

Yang et al. [29] used an objective identification technique (OITREE) for regional extreme events (Ren et al. [33]) to detect the heavy rainfall events which had a larger influencing area and a longer duration than those of the normal precipitation events. They found that more REPEs tended to appear in May and June, particularly for the coastal areas of Guangdong and Guangxi and the mountainous areas in northern Guangxi. Based on the result of Yang et al. [29], we selected the 2-d and 3-d typhoon-free REPEs that occurred in the warm season (May-September) during 1981−2020 (Table 1). In order to examine the general features of the frequency and intensity of these REPEs, we calculated their averaged daily precipitation, and the number of rainfall days. It is clear that, for the average daily precipitation, most stations in Guangdong and Guangxi exceeded 50 mm d^{-1}, with the precipitation above 110 mm d^{-1} mainly situated in the northern part of Guangxi and the coastal areas of Guangdong (Fig. 2). For the rainfall days, most stations in Guangxi and Guangdong exceeded 10 days, with the stations above 25 rainfall days mainly located in the northern Guangxi and the central part of Guangdong.

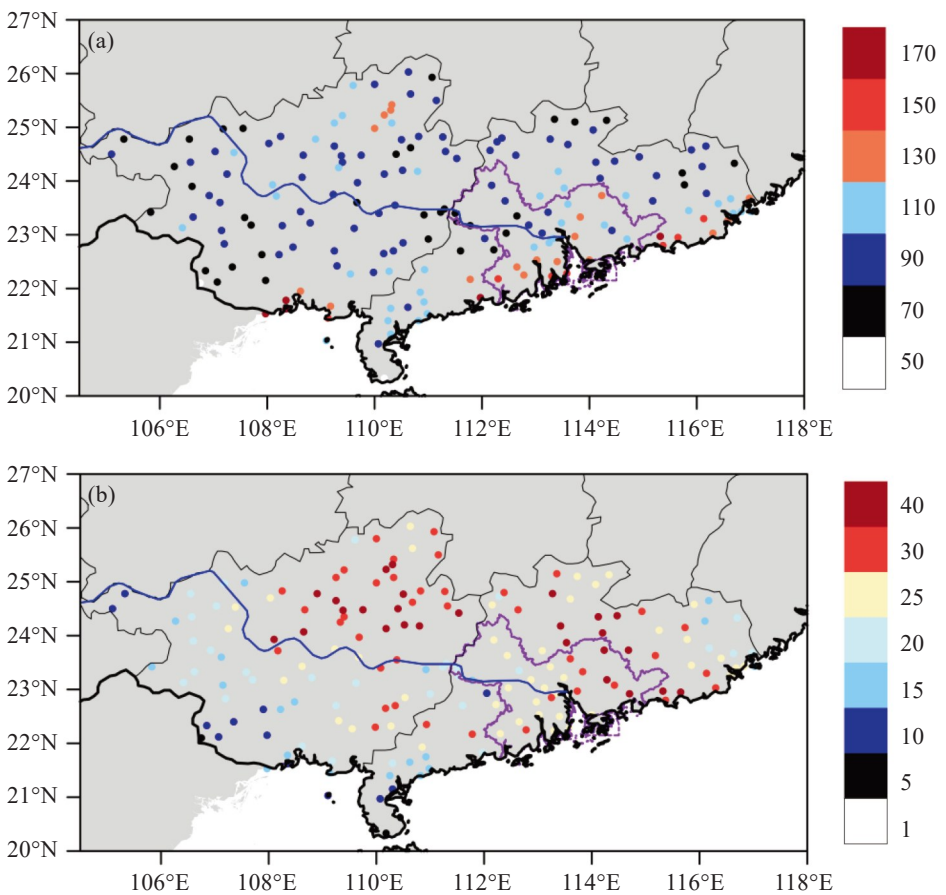

Figure 2. Spatial distribution of (a) average daily precipitation (units: mm d^{-1}) of REPEs and (b) number of REPE days (units: d) over the mainland of south China from May to September during 1981-2020. The Greater Bay Area is outlined in purple.

3.2 *Variations of the wind and precipitation*

In addition to moisture, the steering flow is another key factor that determines the moisture transport. Chen et al. [34] found that diurnal cycles of rainfall are associated with monsoonal southwesterlies over south China. Moreover, the low-level jets, which are defined as the maximum wind zone in the mid - and low-troposphere, often transported abundant moisture to the rainfall regions (Stensrud [35]; Ding [36]; Wen et al. [37]). In this study, we examined the relationship between the spatiotemporal mean wind speed and precipitation. The spatiotemporal mean of the wind speed was calculated as follows: (i) using the ERA5 reanalysis data, we calculated the temporal mean (e.g., if the event lasted for 3 d, the amounts at 0000 UTC of the first, second and third day were averaged as the temporal mean of the 0000 UTC of the 3-d event, etc.) of the 3-dimensional wind speed field during the whole life span of a REPE; (ii) the calculation results of all REPEs were composited with equal weights; and (iii) the results from (ii) were horizontally averaged within the area 18°N−26°N, 111°E−117°E , where low-level jets frequently appeared (Du and Chen [38]). The results of the 2-d REPEs were shown in Fig. 3a, from which it is clear that, the wind featured a

notable diurnal variation with the minimum wind speed present around 1000 UTC−1500 UTC, and the maximum speed around 1900 UTC−2100 UTC. This was consistent with the diurnal variation of the low-level jet (Du and Chen [38]). It should be noted that, during the latter period, strong wind (≥8.5 m s^{-1}) showed the largest thickness around 2100 UTC, which spanned from 850−750 hPa. For the vertical distribution of the wind speed at 2100 UTC (Fig. 3b), it was found that, the wind speed at 775, 800 and 825 hPa were all above 9 m s^{-1}. Similar results could also be found for the 3-d REPEs (not shown). As mentioned above, we used the wind speed averaged at 775, 800 and 825 hPa to represent the relatively strong wind during the REPEs in the following moisture tracking study.

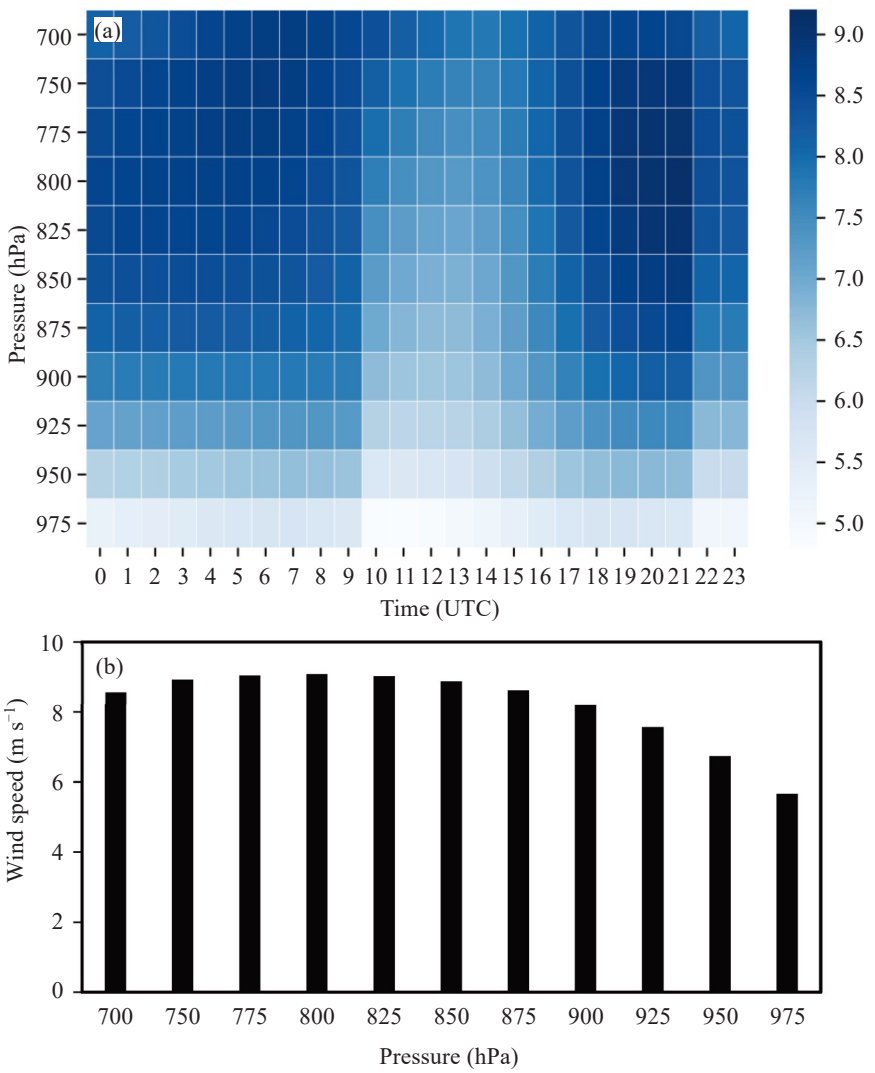

Figure 3. For 2-day REPEs, (a) the diurnal variation of spatiotemporal mean of the wind speed (units: m s^{-1}) at mid- and low-troposphere, and (b) the vertical distribution of spatiotemporal mean of the wind speed (units: m s^{-1}) at 2100 UTC.

To further reveal the relationship between wind and precipitation, the mean of the precipitation was calculated as follows: (i) using the station-observed hourly precipitation, we calculated the temporal mean (the same as that of the calculation of the wind) of the hourly precipitation during the whole life span of a REPE at each station; (ii) the calculation results of all REPEs were composited with equal weights at each station; (iii) the results from (ii) were averaged over all the 176 stations (Fig. 1). The results were shown in Fig. 4. It could be found that, the precipitation intensity of the 3-d REPEs was stronger than that of the 2-d REPEs at each time. The minimum / maximum wind of 2-d REPEs and 3-d REPEs appeared around 1300 UTC / 2100 UTC and 1400 UTC / 2300 UTC, respectively. Similar diurnal variations were found between the wind and the precipitation, with a positive correlation coefficient of 0.91 (2-d events) and 0.87 (3-d events) exceeding the 95% confidence level. This revealed that the REPEs over south China were closely related to the lower-level wind (through transporting moisture, resulting in convergence, etc.). The heights of 775, 800

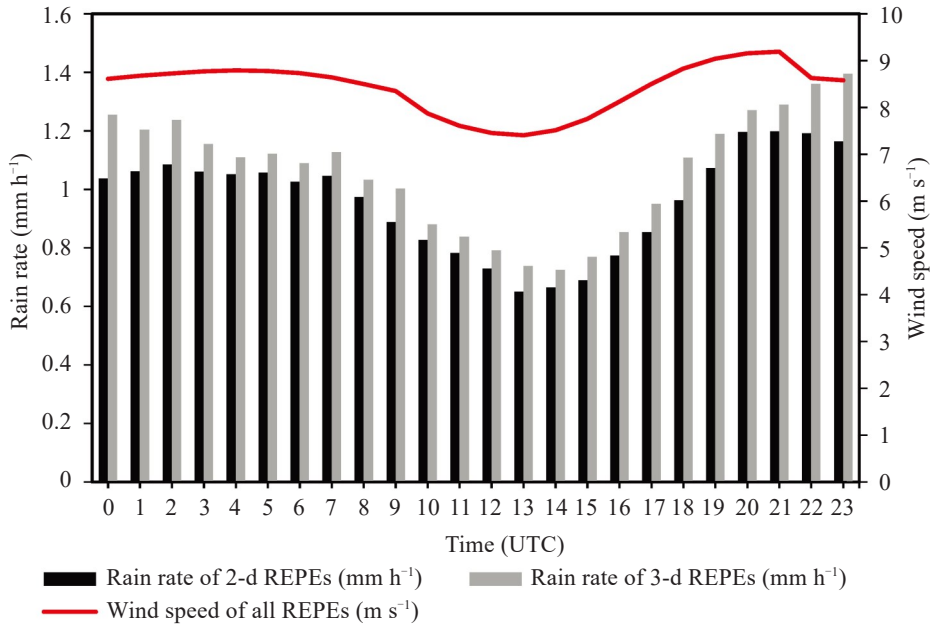

Figure 4. The temporal distribution of spatiotemporal mean of the wind speed (units: m s^{-1}, red line) and the precipitation (units: mm h^{-1}). 2-day REPEs: black bar; 3-day REPEs: gray bar.

and 825 hPa were around 2200 m, 2000 m and 1700 m, respectively and they were used as the initial heights for the backward tracking analyses.

4 MOISTURE TRANSPORTATION CHARACTERISTICS

4.1 *Backward tracking results of two events*

In this section, we used two cases to show how we analyzed the backward tracking results. Two 2-d REPEs from Table 1 were used: 26−27 June 1995 (the first event) and 3−4 August 1995 (the second event). For the first event, all its 528×4 trajectories were shown by the thin black lines in Fig. 5a. Using the cluster method proposed by Stein et al. [31], the 528×4 trajectories were clustered into three groups: Group 1, 2 and 3 (with the proportion of trajectories at 62%, 27%, and 11%, respectively). The moisture contribution rates of Group 1−3 were 41%, 35%, and 24%, respectively. As Groups 1 and 2 both belonged to the SWT, which accounted for an accumulated moisture contribution rate of 76% (Group 3 belonged to the NWT, with a much smaller moisture contribution rate), this event was classified into the SWT-REPE. For the second event (Fig. 5b), its associated 528 × 4 trajectories were also clustered into three groups: Group 1, 2 and 3 (with the proportion of trajectories at 31%, 52%, and 17%, respectively). There were also two groups of trajectories that belonged to the SWT: the moisture contribution rates of Groups 1 and 2 were both 35%. The remaining trajectories (i.e., Group 3) belonged to the SET, accounting for a moisture contribution rate of 30%. Therefore, this event was classified into the SWT-REPE. For both events, the trajectories that belonged to the SWT all passed over the Indochina Peninsula. For the first event, the trajectories that belonged to the NWT mainly transported moisture from the regions in the middle and higher latitudes, whereas for the second event, the trajectories that belonged to the SET mainly transported moisture form the lower latitudes.

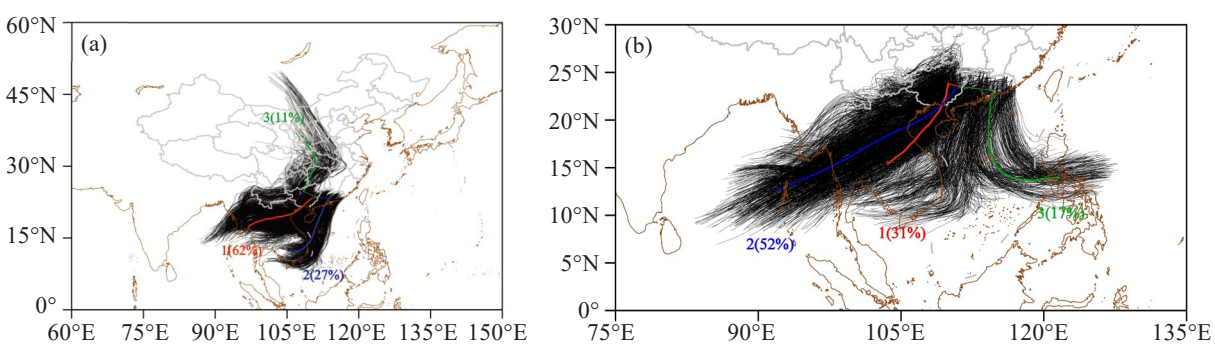

Figure 5. All trajectories (black line) and clustered trajectories for the three groups (red, blue, and green lines) of the two cases, time periods of which were (a) 26-27 June 1995 and (b) 3-4 August 1995, respectively. Colored numbers are the ratios of the trajectory number for Group 1, 2 and 3 to those of all groups (red, blue, and green numbers, respectively).

4.2 *Main features of the moisture transportation*

Similar to the analysis methods mentioned in section 4.1, we analyzed all REPEs and classified the each of them into a specified type according to its dominant moisture contribute rate. In terms of the proportion of trajectories, the ratios of the number of trajectories for the four types (i.e., SWT, NWT, NET and SET) to that for all path types were first calculated for each REPE, and then the ratios were averaged for each type of path. It is shown that the SWT, NWT, NET, and SET accounted for 81%, 6.1%, 2.8% and 10.1% of all trajectories (Fig. 6a), respectively. Based on all trajectories of all REPEs, we calculated the average position of the air particles during the movement for the four types of paths (Fig. 6b). It is clear that, the air particles of the SWT path mainly passed over the Andaman Sea and Indochina Peninsula, those of the NWT the Yunnan-Guizhou plateau, those of the NET the province of Jiangxi, and those of the SET the South China Sea. In terms of the moisture contribution rate, on the basis of Eq. (1), similar to the calculation method of proportion of trajectories, the average moisture contribution rates were calculated for each type of path. The results were presented in Table 2. It can be seen that there were significant differences in the moisture contribution rates for the four types of paths: the path of the SWT possessed the largest contribution rate (>81%), implying that the SWT path was the most important moisture transportation path for the REPEs over south China, and the SET ranked the second, implying the SET path also played an important role in providing moisture for the REPEs over south China. In contrast, the NET had the smallest contribution rate (<3%), and the NWT was the second smallest (<6%). Compared to the moisture contribution rates of the 2-d REPEs, those for the 3-d REPEs were higher in the SWT and NWT (Table 2) but lower in the NET and SET. For the 3-d REPEs, the moisture contribution rate in the SWT path was stronger than that for 2-d REPEs, whereas for the 2-d REPEs, the moisture contribution rate in the SET path was stronger than that for 3-d REPEs (Table 2).

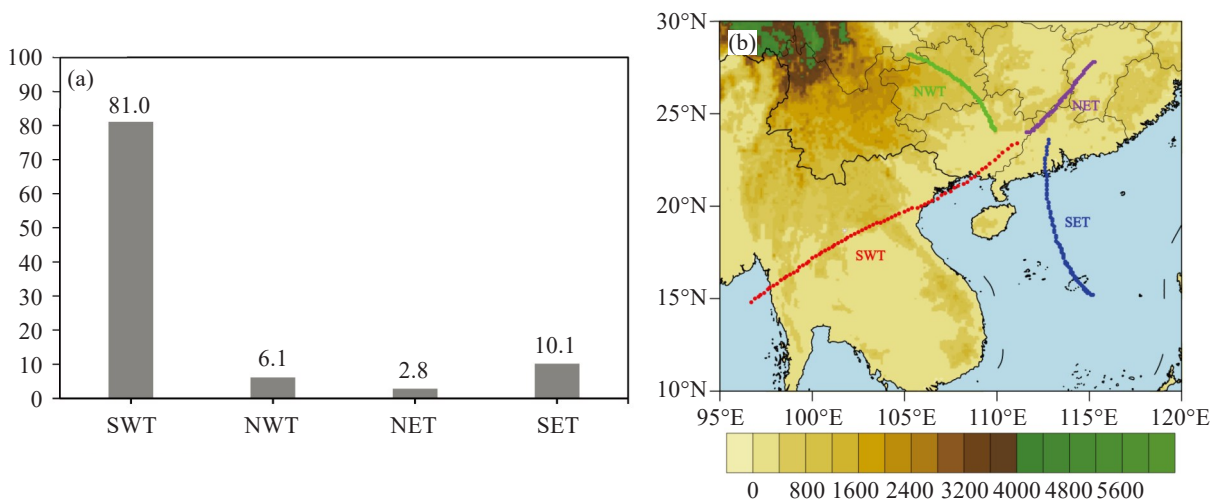

Figure 6. (a) The number ratio (%) of trajectories for the path of a certain type to that for all paths; (b) average positions (color dots) of the air particles during the movement for the four types of paths. The shading indicates the elevations (units: m). SWT=Southwest type, NWT=Northwest type, NET=Northeast type, SET= Southeast type.

Table 2. The moisture contribution rates (%) of the four transport paths.

Types	SWT	NWT	NET	SET
2-day REPEs	81.6	4.9	2.6	10.8
3-day REPEs	84.7	5.6	2.1	7.6
All REPEs	82.4	5.1	2.5	10

*SWT=Southwest type, NWT=Northwest type, NET=Northeast type, SET= Southeast type.

Physical features of the air particles varied notably with space and time during their movements. We further examined the averaged variations of the height, potential temperature, temperature and humidity during the movement of the air particles for the four paths. The average was calculated as follows: for all of the REPEs, all the trajectories (i.e., hourly physical quantities during the backward tracking) that belonged to the SWT were averaged with equal weights to represent the averaged state of the SWT path. Similar processes were taken to get the averages of the other types of paths. The results are presented in Fig. 7.

For the SWT, it had the largest specific humidity (Fig. 7d) and the air particles were nearly saturated or

saturated, as the temperature variation was consistent with that of the specific humidity (Fig. 7c and 7d). These air particles experienced the strongest ascending motion among the four paths (Fig. 7a), and the increase in its potential temperature (Fig. 7b) was also the largest. It should be noted that, from −72 h to −28 h, the height of the SWT increased (Fig. 7a), their specific humidity decreased (Fig. 7d), and their potential temperature increased (Fig. 7b). This indicates that precipitation occurred for the SWT, which could be possibly associated with the heating effect of Indochina Peninsula. The variation of potential temperature ($d\theta/dt$) of the SWT path (Fig. 8) was mainly positive, which indicates that the air particles were affected by the latent heat of precipitation condensation when they passed over Indochina Peninsula. From −28 h to −8 h, the height of the SWT changed slowly (Fig. 7a), and in the mean time their specific humidity increased (Fig. 7d) and potential temperature decreased (Fig. 7b), respectively. This indicates that considerable evaporation appeared. After that, the SWT experienced rapid ascending motion (Fig. 7a), during which the specific humidity reduced (Fig. 7d) and the potential temperature increased (Fig. 7b). This suggests that substantial precipitation occurred again.

For the NWT, it had the smallest specific humidity (Fig. 7d). The relative humidity of these air particles decreased, as their temperature increased and meanwhile their specific humidity changed slowly (Fig. 7c and 7d). There were no obvious variations in the height and potential temperature of these air particles (Fig. 7a and 7b). These air particles experienced the most notable ascending motion from −8 h to 0 h (Fig. 7a), during which their potential temperature and specific humidity changed little (Fig. 7b and 7d). This indicates that the main contribution of the NWT was providing dry cold air for the REPE, which may be related to the topographic blocking effect of the Yunnan-Guizhou Plateau to the west of south China (Shi et al. [39]). For the NET, it had the second largest specific humidity (Fig. 7d). These air particles were nearly saturated or saturated, as their variations in temperature and specific humidity were similar to each other (Fig. 7c and 7d). The NET experienced strong ascending motion from −40 h to 0 h (Fig. 7a), during which its potential temperature increased (Fig. 7b) and specific humidity decreased (Fig. 7d). This indicates that precipitation took place.

For the SET, its specific humidity changed slowly from −72 h to −16 h (Fig. 7d), during which its height also changed slowly (Fig. 7a). After that, from −16 h to 0 h, these air particles experienced notable ascending motion (Fig. 7a), with their potential temperature increased (Fig. 7b) and specific humidity decreased (Fig. 7d). This is a sign that notable precipitation occurred in this period. In order to reveal the specific humidity changes of the air particles as the SET passed over the South China Sea, we calculated the variation of specific humidity (dq/dt) with SET (Fig. 8), and found it had no obvious humidification process when air particles pass through the South China Sea.

As mentioned above, the SWT, NET and SET all experienced notable precipitation, particularly for the period from −8 h to 0 h. In contrast, the NWT showed weaker precipitation, although it also experienced ascending motion from −8 h to 0 h. The key reason for the difference is that the specific humidity of the NWT was much smaller than that of the other three types.

Among all the 87 REPEs over south China during the 40-yr period from 1981 to 2020, there was a total of 80 events (accounting for ~92%) that belonged to the SWT-REPEs (Table 3), with the number of the 2-d events (60) much more than that of the 3-d events (20). For the 2-d events, there were four SET-REPEs, one NWT-REPE and one NET-REPE; whereas for the 3-d events, only one SET-REPEs appeared. The SET-REPEs of 2-d and 3-d events account for ~5.7%, while the NWT-REPE and NET-REPE account for ~2.3%.

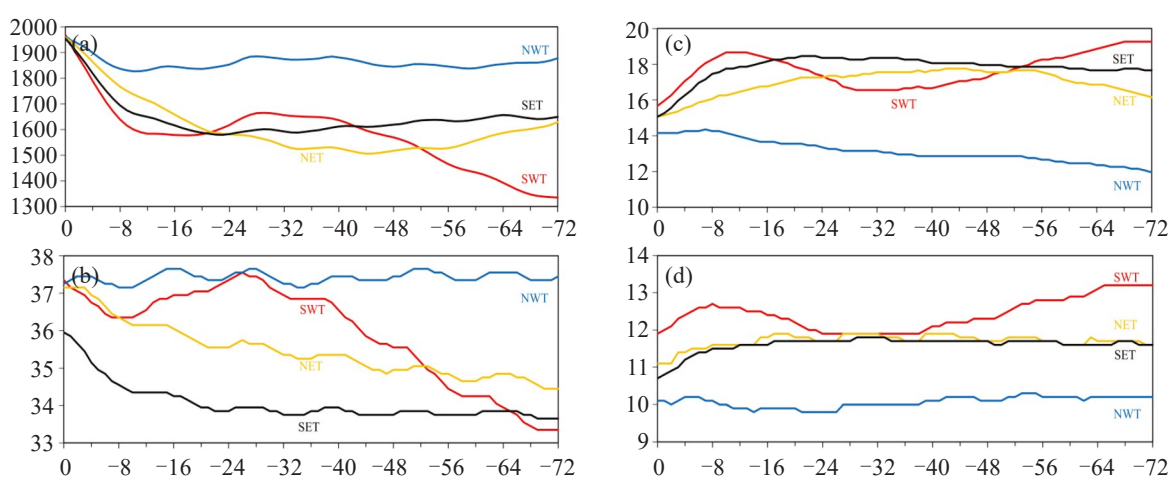

Figure 7. The variations of four physical quantities during the movement of air particles for the four path types, in which the *x*-coordinate is the corresponding backward tracking time. (a) vertical height (m); (b) potential temperature (℃); (c) temperature (℃), and (d) specific humidity (g kg^{-1}). SWT=Southwest type, NWT=Northwest type, NET=Northeast type, SET= Southeast type.

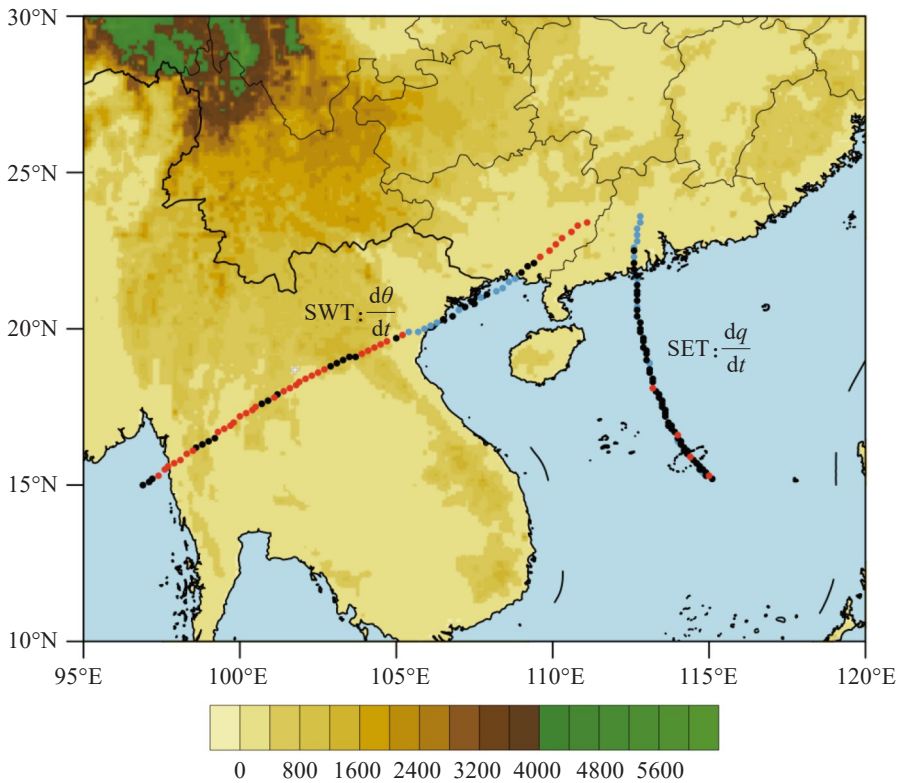

Figure 8. Variations of potential temperature (°C h^{-1}) on the SWT path and specific humidity (g kg^{-1} h^{-1}) on the SET path during the movement of air particles. Red (blue) dots means that $d\theta/dt$ (dq/dt) is positive (negative). Black dot represents that the value is very close to 0. The shading indicates the elevations (units: m).

Table 3. Number of REPEs with the path type of the highest moisture contribution rate belonging to a certain type (i.e., SWT, NWT, NET, and SET).

Types	SWT-REPEs	NWT-REPEs	NET-REPEs	SET-REPEs
2-day REPEs	60	1	1	4
3-day REPEs	20	––	––	1
All REPEs	80	1	1	5

*SWT=Southwest type, NWT=Northwest type, NET=Northeast type, SET= Southeast type. "––" means none. REPEs= Regional extreme precipitation events.

We conducted composite analyses on the moisture flux and their associated divergence from the surface to 300 hPa to understand the differences among the four types of REPEs. The analyses were conducted as follows: (i) using the ERA5 reanalysis data, we calculated the temporal mean of the 3-dimensional wind speed field and specific humidity at each hour (from 0000 UTC to 2300 UTC) during the whole life span of a REPE; (ii) for all the REPEs of the same type (i.e., SWT, NWT, NET, SET), the wind field and specific humidity obtained in (i) were composited with equal weights, which were then used for calculating the moisture flux and their associated divergence from the surface to 300 hPa. It can be seen that, for the SWT-REPEs, the whole region of south China was controlled by strong moisture flux of the southwesterlies and moisture flux convergence (Fig. 9a). For the NWT-REPE, south Guangdong and southeast Guangxi were controlled by strong moisture flux convergence which was mainly due to the convergence of northerly and southwesterly winds (Fig. 9b) because strong northerlies advanced to south China. For the NET-REPE, the moisture flux around south China rotated counterclockwise, which was conducive to the persistent water-vapor convergence in south China (Fig. 9c). For the SET-REPEs, the strong southerly wind between a mesoscale cyclonic circulation around Hainan Island and a notable anticyclonic circulation northeast of Taiwan Island caused an intense moisture transportation and convergence over south China, particularly for the coastal area of Guangdong (Fig. 9d).

5 BACKGROUND CIRCULATION OF REPEs

In order to further examine the key features of the background circulation associated with different types of REPEs, and to clarify their main similarities and

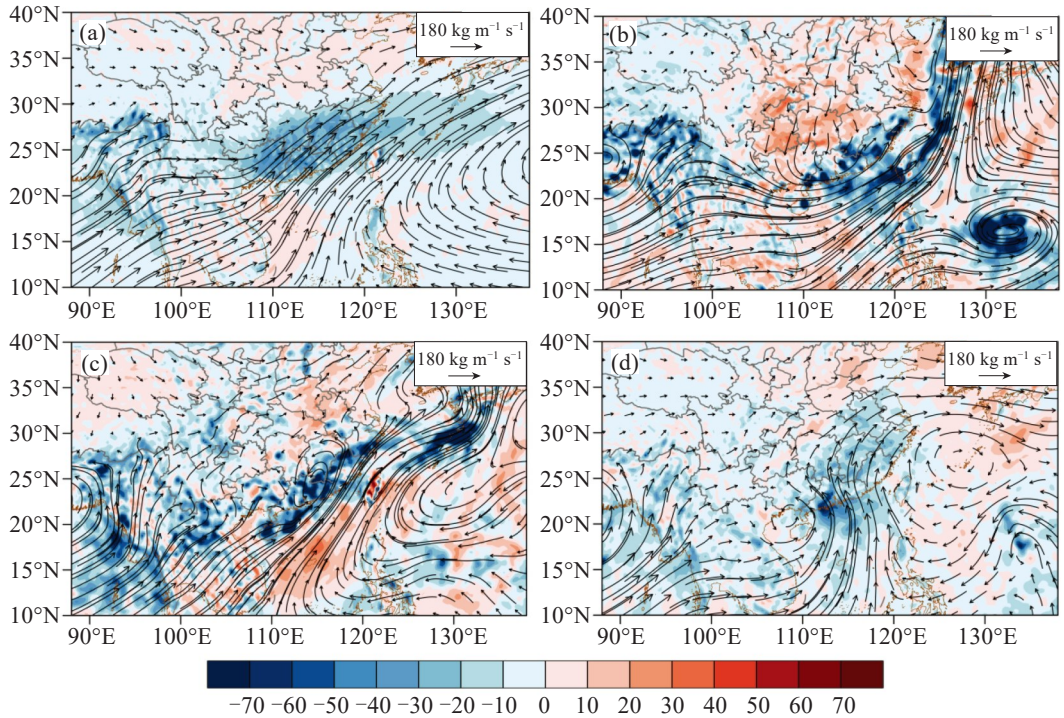

Figure 9. Composite moisture flux (vector; units: kg m^{-1} s^{-1}) and its divergence (shaded; units: 10^{-4} kg m^{-2} s^{-1}) from the surface to 300 hPa of (a) SWT-REPEs, (b) NWT-REPEs, (c) NET-REPEs, and (d) SET-REPEs.

differences, we conducted composite analyses on the four types of REPEs in the middle troposphere (500 hPa) and lower troposphere (800 hPa). These two levels were used because that, the former could effectively reflect the shortwave troughs which affected the REPEs, and the latter was the central level of the moisture transport (Du and Chen [38]; Zhu [40]). The composite analyses on the background circulation were conducted as follows. (i) As the background tracking for a REPE was initiated at 0000 UTC and 1200 UTC on the first and second day (for a 3-d REPE, 0000 UTC and 1200 UTC of the third day were also used to start the background tracking), and ran for 72 h (section 2), for each starting time, we calculated the temporal mean of the background circulation from this start time to 72 h earlier (therefore, for a 2d-REPE, there was four temporal means, and for a 3d-REPE, there was six temporal means). (ii) All the temporal means of a REPE that were obtained from (i) were averaged at 500 hPa or 800 hPa to obtain the composite background circulation for this event. (iii) For all the REPEs of the same type (i. e., SWT, NWT, NET, SET), their composite background circulation obtained in (ii) were composited to generate the final composite background circulation for this REPE type.

The composite 500-hPa background circulation for the four types of REPEs was shown in Fig. 10. For the SWT-REPEs, a relatively warm area (pink shading in Fig. 10a) controlled the lower latitude regions over the northeastern Indian subcontinent, northern Bay of Bengal, southwest China and south China. The warm area featured a weak baroclinity (as the isobars were sparse), with westerly wind dominating it. This caused warm advection, which contributed to promoting ascending motion over south China through the quasi-geostrophic forcing. Trajectories of the SWT were mainly located within this warm area where specific humidity was relatively high. The WPSH was located east of the Philippine islands, and in the middle and high latitudes, there was a weak high ridge around the longitude of 90°E. Overall, the meridional component of the wind in the middle and high latitudes was weak, implying that the cold air was inactive for the SWT-REPEs. From Fig. 11a, it is clear that a strong southwesterly wind band maintained in the lower latitude region, which acted as the most important factor for transporting moisture for the SWT-REPEs. The strong wind was mainly associated with a shortwave trough over the Bay of Bengal, a weak ridge over the Indochina Peninsula, and a shortwave trough over the South China Sea. As Fig. 7d shows, the air particles steered by the strong southwesterly wind mainly experienced two rainfall processes. (i) The first process was from −72 h to −32 h, which appeared when the air particles were located ahead of the shortwave trough over the Bay of Bengal and behind the weak ridge over the Indochina Peninsula (Fig. 11a). Moisture sources for this rainfall were mainly located over the Bay of Bengal. (ii) The second process appeared from −8 h to 0 h (Fig. 7d), when the air particles were mainly located ahead of the shortwave trough over the South China Sea. Moisture sources for this rainfall were mainly located

over the Indochina Peninsula and the South China Sea.

For the NWT-REPE, in the middle and high latitudes, there was a high ridge stretching from Lake Baikal to Gansu province (Fig. 10b); and the WPSH was located over the islands of Japan, which was in a much higher latitude than usual. Between the two systems mentioned above, there was an intense trough in the middle and lower latitudes, behind which a strong northwesterly wind appeared. The northwesterly wind caused a notable cold advection (e. g., reducing the stability of the layer), which acted as a favorable condition for the REPE. At 800 hPa, a nearly meridionally orientated low-pressure band stretched from south China to northeast China (Fig. 11b), with a closed mesoscale vortex center over Guangdong. Northwest of this center, northerly wind was strong, which acted as the most important factor for transporting moisture for the NWT-REPE.

For the NET-REPE, in the middle and high latitudes, a deep trough maintained around the eastern Inner Mongolia (Fig. 10c). In the middle and lower latitudes, the WPSH showed the largest intensity and covering area among all the four types of REPEs. In the lower latitudes, a closed low center appeared south of Guangdong, with a cyclonic wind field controlling south China, which provide favorable conditions for heavy rainfall. At 800 hPa, a near-zonally-orientated strong westerly wind band maintained in the lower latitude region. The strong wind was mainly associated with the shortwave trough over the Bay of Bengal, the weak ridge over the Indochina Peninsula, and the closed mesoscale vortex center over the South China Sea. As Fig. 7d shows, the air particles steered by the strong wind mainly experienced precipitation from −16 h to 0 h. The moisture source for this rainfall was mainly located over the Bay of Bengal and South China Sea (Fig. 11c).

For the SET-REPEs, in the middle and high latitudes, the meridional wind was much smaller than the zonal wind (Fig. 10d). In the lower latitudes, there was a shortwave trough south of the Tibetan Plateau, and the isobars were sparse, implying that the baroclinity was weak. The WPSH showed the smallest covering area among the four types of REPEs, whereas, its western boundary was also the closest to south China. Southerly wind around the western boundary of the WPSH induced warm advection (not shown), which helped to promote ascending motion. At 800 hPa, there was a transversal trough that stretched from the South China Sea to the Indochina Peninsula (Fig. 11d). South of the transversal trough, westerly wind maintained a strong intensity, and northeast of the transversal trough, southeasterly wind was strong. The latter acted as the most important factor for transporting moisture for the SET-REPEs, with the South China Sea being the main moisture source.

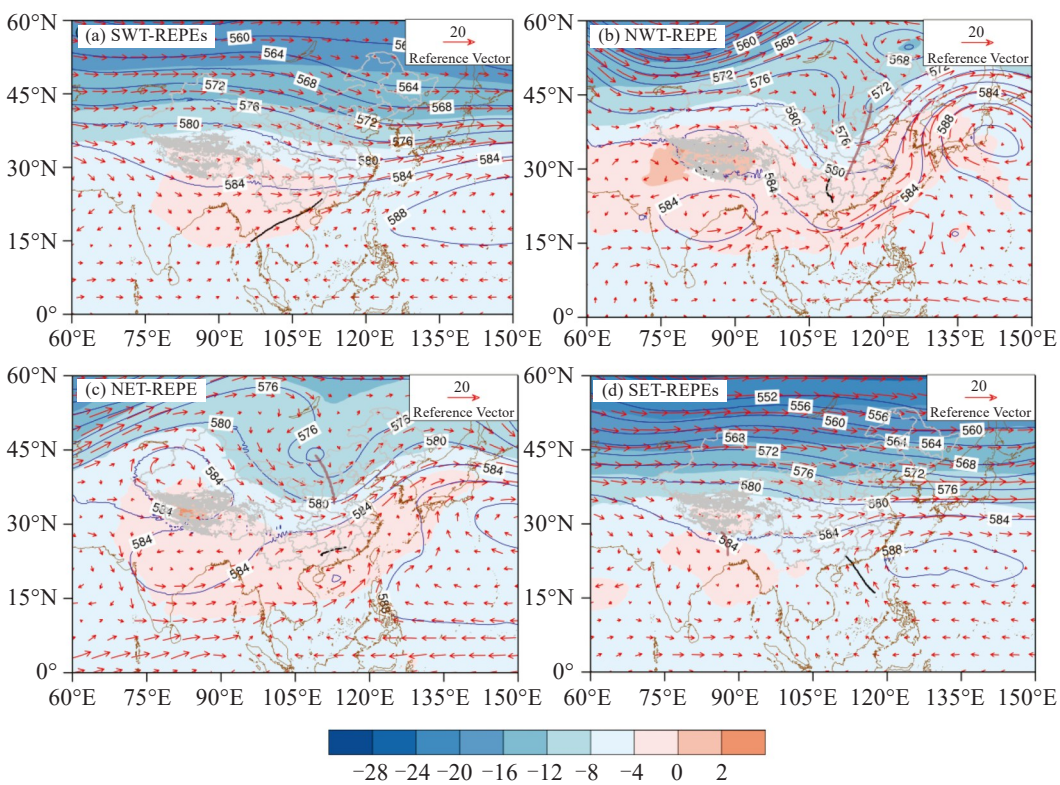

Figure 10. Composite temperature (color shaded, units; ℃), wind (red arrow, units: m s^{-1}), and geopotential height (blue line, units: dagpm) of (a) SWT-REPEs, (b) NWT-REPE, (c) NET-REPE, and (d) SET-REPEs at 500 hPa. The thick solid black line represents the average position of the air particles during the movement. The brown solid line represents the trough. SWT=Southwest type, NWT=Northwest type, NET=Northeast type, SET= Southeast type.

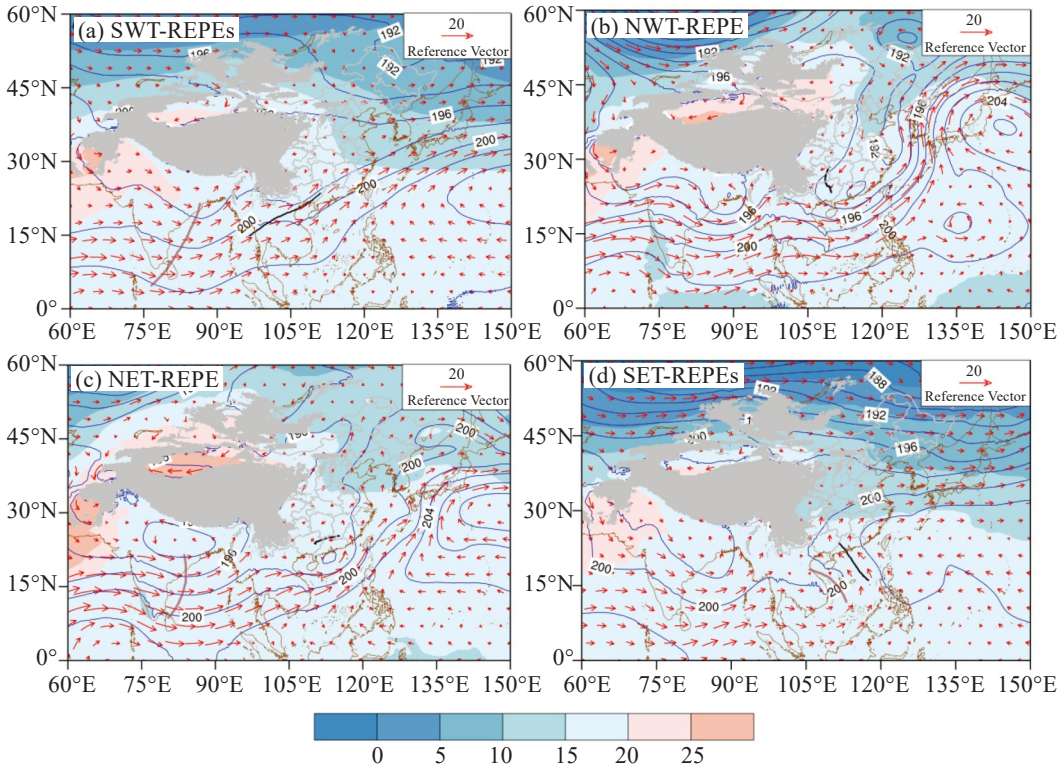

Figure 11. As Fig. 7, but for 800 hPa.

6 CONCLUSION AND DISCUSSION

In this study, based on statistical analyses on the REPEs over south China during a 40-yr period from Yang et al. [29], we applied backward tracking analyses on the 2-d and 3-d REPEs by using the HYSPLIT V4.9 model to determine the main moisture transport paths for these REPEs and conducted composite studies on the background circulation associated with the moisture transport to determine the dominant weather systems that controlled the transport. Through these, the universal characteristics of the moisture transport of the REPEs over south China and the key features of their associated background circulation were shown. Main findings are obtained as follows.

(1) The wind that transported moisture for the REPEs over south China featured a notable diurnal variation (with the minimum speed present around 1000 UTC-1500 UTC, and the maximum speed around 1900 UTC-2100 UTC), which were consistent with the diurnal variations of the precipitation.

(2) A total of four types of REPEs could be determined according to the relative importance of the moisture contribution rates of different paths, among which the SWT-REPEs occupied a proportion of ~92%, the SET-REPEs accounted for ~5.7%, and the remaining two types both had a contribution of ~2.3%.

(3) Trajectory analyses indicate that, for the SWT, the air particles possessed the largest specific humidity and experienced the most intense ascending motion; for the NET and SET, their specific humidity and ascending motion were similar to each other (all ranked second), whereas for the NWT, their specific humidity was the smallest and ascending motion was the weakest. This explained why precipitation intensity was the strongest/weakest for the SWT/NWT-REPEs among the four types of REPEs. South China was dominated by notable moisture flux convergence for the four types of REPEs, but their moisture fluxes were transported by different flows from each other remarkably.

(4) Composite analyses show that the background circulation of four types of REPEs differed from each other remarkably. For the SWT-REPEs, the isohypses were sparse over south China, and the WPSH was located east of the Philippine islands. Their moisture transport was mainly driven by a strong lower-tropospheric southwesterly wind band which was associated with the shortwave trough over the Bay of Bengal, the weak ridge over the Indochina Peninsula, and the shortwave trough over the South China Sea. Moisture sources for this type of REPEs were mainly located over the Indochina Peninsula and the South China Sea. For the SET-REPEs, they showed a similar 500-hPa composite background circulation to that of the SWT-REPEs, except that, the WPSH was much weaker and closer to south China. Their moisture transport was mainly steered by the strong lower-tropospheric southeasterly wind northeast of a transversal trough that stretched from the South China Sea to the Indochina Peninsula. The South China Sea was the main moisture source for this type of REPEs. For the NWT-REPE and NET-REPE, there were a strong trough and a notable

cyclonic circulation at 500 hPa, respectively. Their moisture transport was mainly driven by the cyclonic wind field associated with mesoscale vortices in the lower troposphere (the mesoscale vortex for the NWT-REPE was located in higher latitudes than that of the NET-REPE).

***Acknowledgements*:** We would like to acknowledge the China Meteorological Administration for providing the precipitation data used in this study.

REFERENCES

[1] LI D S, SUN J H, FU S M, et al. Spatiotemporal characteristics of hourly precipitation over central eastern China during the warm season of 1982–2012 [J]. International Journal of Climatology, 2015, 36(8): 3148-3160, https://doi.org/10.1002/joc.4543

[2] FU S M, LI D S, SUN J H, et al. A 31-year trend of the hourly precipitation over South China and the underlying mechanisms [J]. Atmospheric Science Letters, 2016, 17(3): 216-222, https://doi.org/10.1002/asl.645

[3] ALEXANDER L V. Global observed long-term changes in temperature and precipitation extremes: A review of progress and limitations in IPCC assessments and beyond [J]. Weather and Climate Extremes, 2016, 11: 4-16, https://doi.org/10.1016/j.wace.2015.10.007

[4] WANG X Y, LI Y Q, YAN M, et al. Changes in temperature and precipitation extremes in the arid regions of China during 1960-2016 [J]. Frontiers in Ecology and Evolution, 2022, 10: 902813, https://doi. org / 10.3389 / fevo.2022.902813

[5] CHENG S Y, XU L R, QIN W, et al. Temporal and spatial variation of extreme precipitation in the Longchuan River Basin in 1978-2015 years [J]. IOP Conference Series: Earth and Environmental Science, 2018, 208(1): 012026, https://doi.org/10.1088/1755-1315/208/1/012026

[6] CAO X G, ZHANG J, WANG H, et al. Analysis on a severe convective rainstorm hitting Shanghai on 25 August 2008 [J]. Meteorological Monthly (in Chinese), 2009, 35 (4): 51-58, https://doi. org / 10.7519 / j. issn. 1000-0526.2009.04.007

[7] ZHANG J Y, SHI Y, WANG Q H, et al. Numerical simulation and analysis of a heavy rain process [J]. Journal of Marine Meteorology (in Chinese), 2006, 26(104): 22-25, https://doi.org/10.19513/j.cnki.issn1005-0582.2006.01.006

[8] WANG T, WEI K, MA J. Atmospheric rivers and mei-yu rainfall in China: A case study of summer 2020 [J]. Advances in Atmospheric Sciences, 2021, 38(12): 2137-2152, https://doi.org/10.1007/s00376-021-1096-9

[9] ZHUANG X C, LI B Y, ZHAO J W, et al. Water vapor source and transport characteristics of rainstorm processes in warm season on southern slope of the Tianshan Mountains [J]. Journal of Arid Meteorology (in Chinese), 2022, 40(1): 30-40, https://doi. org / 10.11755 / j. issn. 1006-7639(2022)-01-0030

[10] ZHOU C Y, LI Y Q, LI W, et al. Climatological characteristics of water vapor transport over East Asian and water vapor source in autumn [J]. Journal of Tropical Meteorology (in Chinese), 2006, 22(4): 380-385.

[11] ZHANG X M, JIANG Z H, LIU X D, et al. The characteristics of east-Asia vapor transportation in summer [J]. Journal of Tropical Meteorology (in Chinese), 2009, 25(6): 733-739.

[12] LI X Z, LIANG W, WEN Z P. Characteristics of atmospheric water vapor and its relationship with rainfall in South China in Northern autumn, winter and spring [J]. Journal of Tropical Meteorology (in Chinese), 2010, 26 (5): 626-632, https://doi. org / 10.3969 / j. issn. 1004-4965.2010.05.016

[13] LIN A L, GU D J, ZHENG B, et al. Anomalous transport of water vapor for sustained torrential rain and its variation [J]. Journal of Tropical Meteorology (in Chinese), 2014, 30(6): 1001-1010, https://doi.org/10.3969/j.issn.1004-4965.2014.06.001

[14] ZHOU T J, YU R C. Atmospheric water vapor transport associated with typical anomalous summer rainfall patterns in China [J]. Journal of Geophysical Research, 2005, 110(D8): D08104, https://doi. org / 10.1029 / 2004JD005413

[15] SHEN L L, HE J H, ZHOU X J, et al. The regional variabilities of summer rainfall in China and its relation with anomalous moisture transport during the recent 50 years [J]. Acta Meteorologica Sinica (in Chinese), 2010, 68(6): 918-931, https://doi.org/10.11676/qxxb2010.087

[16] HU P, ZHANG Z S, QIAO S B, et al. The interdecadal variation and physical mechanism for the summertime water vapor transport in northern east Asia in the late 1990s [J]. Chinese Journal of Atmospheric Sciences (in Chinese), 2016, 40(5): 933-945, https://doi.org/10.3878/j.issn.1006-9895.1512.15158

[17] HU Y Y, ZHANG Z Y, JIAN M Q, et al. Variation of summer meridional water vapor transport over east Asia and its impact on extreme precipitation [J]. Journal of Tropical Meteorology (in Chinese), 2020, 36(6): 784-794, https://doi.org/10.16032/j.issn.1004-4965.2020.070

[18] MAO C Y, GONG L Q, LIAO J Y, et al. Analysis of the characteristics of a regional heavy rain in Zhejiang province in June 2016 [J]. Guangdong Meteorology (in Chinese), 2018, 40(5): 27-30, https://doi. org / 10.3969 / j. issn.1007-6190.2018.05.007

[19] WANG M M, WEI M, WANG H, et al. An analysis of the characteristics of the water vapor during a persistent rainstorm event in Chengdu [J]. Transactions of Atmospheric Sciences (in Chinese), 2018, 41(6): 861-871, https://doi.org/10.13878/j.cnki.dqkxxb.20160410012

[20] TAO S Y. Torrential Rain in China [M]. Beijing: Science Press, 1980: 225 (in Chinese).

[21] ZHAO S X, TAO Z Y, SUN J H, et al. Analysis Study on Mechanism of Meiyu Front Rainstorm in Yangtze River Basin [M]. Beijing: China Meteorological Press, 2004: 281 (in Chinese).

[22] TAN Z M, ZHAO S X, SUN J H, et al. Study on Structure and Mechanism of Meso - β Scale Severe Convection System over South China [M]. Beijing: China Meteorological Press, 2013: 266 (in Chinese).

[23] CHEN J, PANG B, WU Z Q, et al. Evaluation of final-scale precipitation forecast of GRAPES_Meso 3 km convective-scale model in early summer rainy season in South China under complex topographical conditions [J]. Transactions of Atmospheric Sciences (in Chinese), 2022, 45(1): 99-111, https://doi. org / 10.13878 / j. cnki. dqkxxb.20210308001

[24] WANG S R, ZHU C M, CHENG L, et al. The Global

Water Cycle and Water Resources [M]. China Meteorological Press, 2003: 93-95 (in Chinese).

[25] YU B, LIN Y H, CHEN J Y, et al. Vapor source characteristics of precipitation in South China during May [J]. Climatic and Environmental Research (in Chinese), 2014, 19(4): 507-514, https://doi.org/10.3878/j.issn.1006-9585.2014.12195

[26] LI X F, TANG Z F, YANG T, et al. Study on water vapor transport characteristics of low frequency precipitation in South China during Pre-flood seasons [J]. Meteorology and Disaster Reduction Research (in Chinese), 2017, 40 (2) :83-91, https://doi.org/10.12013/qxyjzyj2017-013

[27] HU L, HE J H, GAO S T. An analysis of large-scale condition for persistent heavy rain in South China [J]. Journal of Nanjing Institute of Meteorology (in Chinese), 2007, 30(3): 345-351.

[28] JI Z P, GU D J, WU N G, et al. Variations of torrential rain in first rainy season in Guangdong province and its relationships with the biweekly oscillation of 500 hPa key region [J]. Journal of Applied Meteorological Science (in Chinese), 2010, 21(6): 671-684.

[29] YANG W T, SUN J H, FU S M, et al. Study on regional extreme precipitation events over mainland of the South China during 1981-2020 [J]. Chinese Journal of Atmospheric Sciences (in Chinese), in Press, https://doi.org/10.3878/j.issn.1006-9895.2211.22056

[30] HERSBACH H, BELL B, BERRISFORD P, et al. The ERA5 global reanalysis [J]. Quarterly Journal of the Royal Meteorological Society, 2020, 146(730): 1999-2049, https://doi.org/10.1002/qj.3803

[31] STEIN A F, DRAXLER R R, ROLPH G D, et al. NOAA's HYSPLIT atmospheric transport and dispersion modeling system [J]. Bulletin of the American Meteorological Society, 2015, 96(12): 2059-2077, https://doi.org/10.1175/BAMS-D-14-00110.1

[32] SUN J H, WANG H J, WEI J, et al. The sources and transportation of water vapor in persistent heavy rainfall events in the Yangtze-Huaihe River Valley [J]. Acta Meteorologica Sinica (in Chinese), 2016, 74(4): 542-555, https://doi.org/10.11676/qxxb2016.047

[33] REN F M, CUI D L, GONG Z Q, et al. An objective identification technique for regional extreme events [J]. Journal of Climate, 2012, 25(20): 7015-7027, https://doi.org/10.1175/JCLI-D-11-00489.1

[34] CHEN G X, LAN R Y, ZENG W X, et al. Diurnal variations of rainfall in surface and satellite observations at the monsoon coast (South China) [J]. Journal of Climate, 2018, 31 (5): 1703-1724. https://doi.org/10.1175/JCLI-D-17-0373.1

[35] STENSRUD D J. Importance of low-level jets to climate: A review [J]. Journal of Climate, 1996, 9(8): 1698-1711, https://doi. org / 10.1175 / 1520-0442(1996)009<1698: IOLLJT>2.0.CO;2

[36] DING Y H. Advanced Synoptic Meteorology (The Second Edition) [M]. Beijing: China Meteorological Press, 2008 (in Chinese).

[37] WEN P, XU Y L, LIU L S. Analysis on mechanism of torrential rain in South China induced by Typhoon MANGKHUT (2018) [J]. Journal of Marine Meteorology (in Chinese), 2019, 39(3): 29-35, https://doi.org/10.19513/j.cnki.issn2096-3599.2019.03.004

[38] DU Y, CHEN G X. Climatology of low-level jets and their impact on rainfall over southern China during early-summer rainy season [J]. Journal of Climate, 2019, 32 (24): 8813-8833, https://doi. org / 10.1175 / JCLI-D-19-0306.1

[39] SHI Z G, SHA Y Y, LIU X D, et al. Effect of marginal topography around the Tibetan Plateau on the evolution of central Asian arid climate: Yunnan-Guizhou and Mongolian Plateaus as examples [J]. Climate Dynamics, 2019, 53(7): 4433-4445, https://doi.org/10.1007/s00382-019-04796-z

[40] ZHU Q G. Principles and Methods of Meteorology (4th Edition) [M]. Beijing: China Meteorological Press, 2007 (in Chinese).

Citation: YANG Wen-ting, FU Shen-ming, SUN Jian-hua, et al. Moisture Transport and Associated Background Circulation for the Regional Extreme Precipitation Events over South China in Recent 40 Years [J]. Journal of Tropical Meteorology, 2023, 29(1): 101-114, https://doi.org/10.46267/j.1006-8775.2023.008